^{48}V: An experimental and theoretical paradigm in the middle of the $1f_{7/2}$ shell

F. Brandolini,[1] N. Mărginean,[2,3] S. Hankonen,[4] N. H. Medina,[5] R. V. Ribas,[5] J. Sanchez-Solano,[6] S. M. Lenzi,[1] S. Lunardi,[1] D. R. Napoli,[2] A. Poves,[6] C. A. Ur,[1,3] D. Bazzacco,[1] G. de Angelis,[2] M. De Poli,[2] E. Farnea,[2] A. Gadea,[2] T. Martínez,[2] and C. Rossi-Alvarez[1]

[1]*Dipartimento di Fisica dell' Università and INFN, Sezione di Padova, Padova, Italy*

[2]*Laboratori Nazionali di Legnaro-INFN, Legnaro, Italy*

[3]*Institute of Physics and Nuclear Engineering, Bucharest, Romania*

[4]*Department of Physics, Jyvaskyla, Finland*

[5]*Instituto de Fisica, Universidade de São Paulo, São Paulo, Brazil*

[6]*Departamento de Física Teorica, Universidad Autónoma, Cantoblanco, Madrid, Spain*

(Received 12 November 2001; published 1 August 2002)

An extensive spectroscopic study of ^{48}V has been performed using fusion-evaporation reactions to deduce the decay scheme and to measure transition probabilities through the Doppler shift attenuation method. Experimental levels were grouped into five bands, labeled with Nilsson configurations. Bands become nearly spherical approaching band termination. Large-scale shell model calculations were performed, producing results in very good agreement with the experimental data.

DOI: 10.1103/PhysRevC.66.024304 PACS number(s): 21.10.Tg, 23.20.Lv, 27.40.+z

I. INTRODUCTION

A very interesting situation of the coexistence of spherical and deformed shapes was discovered recently in nuclei in the middle of the $1f_{7/2}$ shell, in a series of experiments performed at the Legnaro National Laboratories using the γ spectrometer GASP. New information on ^{48}Cr [1,2], ^{50}Cr [2], ^{49}Cr [3,4], ^{47}V [4], and ^{46}V [5] was obtained. An essential part of this scientific program was the measurement of $B(E2)$ and $B(M1)$ strengths, in order to investigate collective effects and single-particle features, respectively. For this purpose Doppler shift attenuation method (DSAM) lifetimes were deduced for many levels using the narrow gate on transition below (NGTB) procedure, which avoids the systematic errors due to side feeding [6]. Our attention was focused on the yrast sequence of levels of both natural and unnatural parities up to the band termination in $1f_{7/2}^{n}$ and $1d_{3/2}^{-1} \otimes 1f_{7/2}^{n+1}$ configuration space, respectively. Prolate or triaxial deformation is built at low spin, evolving towards a spherical shape approaching the band termination.

All of the observed features of the natural-parity levels were described successfully by large-scale shell model (LSSM) calculations in full *fp* configuration space [7–11]. Good agreement was also obtained for the negative-parity levels by including a $1d_{3/2}$ hole into the configuration space.

It is a natural evolution after discussing the even-even cases ^{48}Cr and ^{50}Cr and the odd-*A* cases ^{49}Cr and ^{47}V to extend our comparison to odd-odd nuclei. Odd-odd nuclei may provide quite a stringent test for LSSM calculations, because of their particular sensitivity to proton-neutron residual interactions.

The $N=Z$ nucleus ^{46}V has been recently studied [5]. ^{48}V proved itself to be richer in experimental information owing to its strong population in fusion-evaporation reactions, providing complementary information to ^{46}V.

The available experimental information on the nucleus ^{48}V was scarce. The dipole ground-state (g.s.) band was known up to spin/parity 13^+, except for the 10^+ and 12^+ levels [12]. No relevant new experimental data have been reported in the last ten years, save for two tentative levels at 8285 keV and 8584 keV excitation energy with assignments (14^+) and (15^+), respectively [13]. The low-spin levels of the g.s. band can be interpreted as built on a $K^\pi=4^+$ bandhead generated by parallel coupling of the $\pi[321]3/2^-$ and $\nu[312]5/2^-$ Nilsson orbitals. Recently, the existing experimental data have been compared with shell model calculations in $f_{7/2}$, $p_{3/2}$, $p_{1/2}$ configuration space [14].

The low-lying negative-parity levels were grouped in two bands with $K^\pi=1^-$ and $K^\pi=4^-$ up to spins 6^- and 8^-, respectively [12]. These bands are interpreted to be generated by the parallel and antiparallel couplings of a $\pi[202]3/2^+$ orbital, from the $1d_{3/2}$, with a $\nu[312]5/2^-$ orbital, following the excitation from the weakly bound $\pi[202]3/2^+$ orbital to the $\pi[321]3/2^-$ one. Lifetime measurements were previously reported only for some low-lying states [12].

II. EXPERIMENTAL PROCEDURE

The present study of ^{48}V was performed using both thin (self-supporting) and thick (backed) targets. In the first experiment, the reaction ^{24}Mg on ^{28}Si at a 100 MeV beam energy was used. The target consisted of a 0.4 mg/cm^2 ^{28}Si foil. The $3p1n$ evaporation channel leading to ^{48}V was estimated from the present data to have about 25% of the total fusion cross section. Gamma rays were detected with the GASP array, composed of 40 Compton-suppressed HPGe detectors and of an 80-element BGO ball acting as a γ-ray multiplicity filter. Light charged particles were detected with the ISIS array, composed of 40 ΔE-E Si telescopes. Events were stored on tape when at least two Ge detectors and two elements of the multiplicity filter fired in coincidence. Since the beam intensity had to be limited because of the high counting rate in the most forward elements of ISIS, we decided to perform the second experiment using GASP only.

In the second measurement, the inverse reaction ^{28}Si on ^{24}Mg at 115 MeV beam energy was employed, thus populating the ^{52}Fe compound nucleus at the same excitation energy as in the first experiment. The beam time was divided in two parts, using a 0.8 mg/cm^2 target backed with 15 mg/cm^2 of gold and lead, respectively. The trigger condition was the same as the previous experiment.

In both experiments, energy and efficiency calibrations were performed with standard radioactive sources of ^{152}Eu, ^{56}Co, and ^{60}Co, as well as with firmly assigned narrow lines in ^{48}V [12].

III. EXPERIMENTAL RESULTS FOR THE LEVEL SCHEME

The level scheme of the nucleus ^{48}V deduced from the present work is shown in Fig. 1. The high-spin part of the decay scheme has been extended mainly using the data set from the thin target measurement, using a γ-γ-γ coincidence cube and a γ-γ matrix requiring the coincidence with three protons detected in the ISIS array.

A total of 24 new levels were observed and 25 new lifetimes were determined. Observed levels are grouped in five bands. The ground-state band is extended up to the band termination in $1f_{7/2}^{n}$ space at $I^{\pi}=15^{+}$. The $K^{\pi}=1^{-}$ band is extended up to $I^{\pi}=8^{-}$. Two new structures were observed. The band identified with $K^{\pi}=1^{+}$, which includes already known low-spin levels up to $I^{\pi}=5^{+}$, has been extended up to $I^{\pi}=13^{+}$. The band labeled with $K^{\pi}=8^{-}$ is enterely new and is observed up to the band terminating state $I^{\pi}=17^{-}$ in the $1d_{3/2}^{-1}\otimes 1f_{7/2}^{n+1}$ space.

In Fig. 2 we show some examples of gated γ spectra, obtained from the γ-γ matrix. Unless differently stated, identified lines belong to ^{48}V. In Fig. 2(a) the spectrum is obtained by gating on the $6^{+}\rightarrow 4^{+}$ and $7^{+}\rightarrow 5^{+}$ transitions, both of 627 keV. All transitions of the yrast band, as well as several transitions belonging to other bands, are observed with high statistics, which allowed cross-coincidence checks. The experimental levels to which we assign $I^{\pi}=14^{+}$,15^{+} are in disagreement with those reported in Ref. [13], where the statistics were much lower.

In Fig. 2(b) the high-spin part of the $K^{\pi}=8^{-}$ band is shown by gating on the $15^{-}\rightarrow 13^{-}$ 2505 keV transition. The other signature of the same band is better observed in Fig. 2(c) with a gate on the $8^{-}\rightarrow 7^{-}$ 806 keV transition, which also includes some contribution from the $10^{-}\rightarrow 9^{-}$ 808 keV transition.

The thin target data were complemented at low energies with data from the thick target experiment which were further used for lifetime measurements, providing also parity assignments for the new high-spin levels. In Table I we present the results for the ground-state band, while those for the remaining positive-parity levels are shown in Table II. The values for negative-parity levels are shown in Table III and those for the $E1$ linking transitions connecting the bands are presented in Table IV. Branching ratios were deduced by gating on a feeding transition, while for the intensities the gate was set on lower transitions.

The second positive-parity structure, weakly populated and labeled with ''*s*'' in Fig. 1, is composed of levels with spins ranging between 1^{+} and 13^{+}. This side structure is yrast at low spin. It is classified as the $K^{\pi}=1^{+}$ band generated by the antiparallel coupling of the $\pi[321]3/2^{-}$ and $\nu[312]5/2^{-}$ orbitals. A large signature splitting is observed. The $B(M1)$ values for the transitions from the lower part of the band towards the yrast states are in general much smaller compared to the intraband transitions. Actually, intense intraband $M1$ transitions are observed in spite of their lower energy compared to the $M1$ transitions connecting to the g.s. band. The most enhanced interband transition is the $5_{s}^{+}\rightarrow 6^{+}$ of 637 keV, which is a factor of 4 retarded with respect to the $5_{s}^{+}\rightarrow 4_{s}^{+}$ 651 keV intraband transition. While a K classification for this band appears reasonable at low spin, in spite of the large signature splitting, this is not the case for the almost spherical high-spin states.

Concerning the negative-parity levels, to distinguish the two previously known bands classified as $K^{\pi}=4^{-}$ and $K^{\pi}=1^{-}$, the members of the latter are labeled with ''*s*'' in Table III. The bands are well characterized, but they are connected by a rather strong $7_{s}^{-}\rightarrow 6^{-}$ $M1$ transition, suggesting a configuration mixing between the two 7^{-} levels. Only branching ratios not changing the parity are reported in Table III.

The yrare 8^{-} level is observed at 4073 keV excitation energy. An 8^{-} state is expected to be the bandhead of a $K^{\pi}=8^{-}$ band generated by the excitation of a proton from the $[202]3/2^{+}$ orbital to the empty $[312]5/2^{-}$ one and by the parallel coupling of the four unpaired nucleons. The two lowest 8^{-} states at 3980 and 4073 keV excitation energy have similar decay properties, pointing to a strong mixing between them, due to their small excitation energy difference. This can be described with a crossing of the $K^{\pi}=4^{-}$ and $K^{\pi}=8^{-}$ bands. After the crossing the $K^{\pi}=8^{-}$ band further develops and is labeled with ''*t*'' in Table III. Both signatures of this band are observed up to the band termination in the $d_{3/2}^{-1}\otimes f_{7/2}^{n+1}$ space at 17^{-} and are connected by strong $E2$ transitions, as shown by lifetime measurements.

No $E2$ transition connecting the 10^{-} level to the two lower 8^{-} levels is observed. This could be partially explained considering that in a rotor description the stretched $E2$ transition decaying to the bandhead is strongly retarded, but configuration mixing has to be considered too.

IV. LSSM CALCULATIONS

Large-scale shell model calculations in the full *pf* configuration space for the positive-parity levels were performed with the code ANTOINE [7], using the KB3G residual interaction [15]. The predictions obtained with this residual interaction differ only little in the present case from those using the KB3 interaction, reported in previous articles [2–4]. In Fig. 3 a full comparison of both the experimental yrast and yrare bands with the LSSM predictions is shown. The agreement is excellent in spite of the complexity of the level scheme.

Calculations have been performed also for the negative-parity states, allowing a hole in the $1d_{3/2}$ orbital and allowing up to three nucleons to be excited from the $1f_{7/2}$ orbital. As

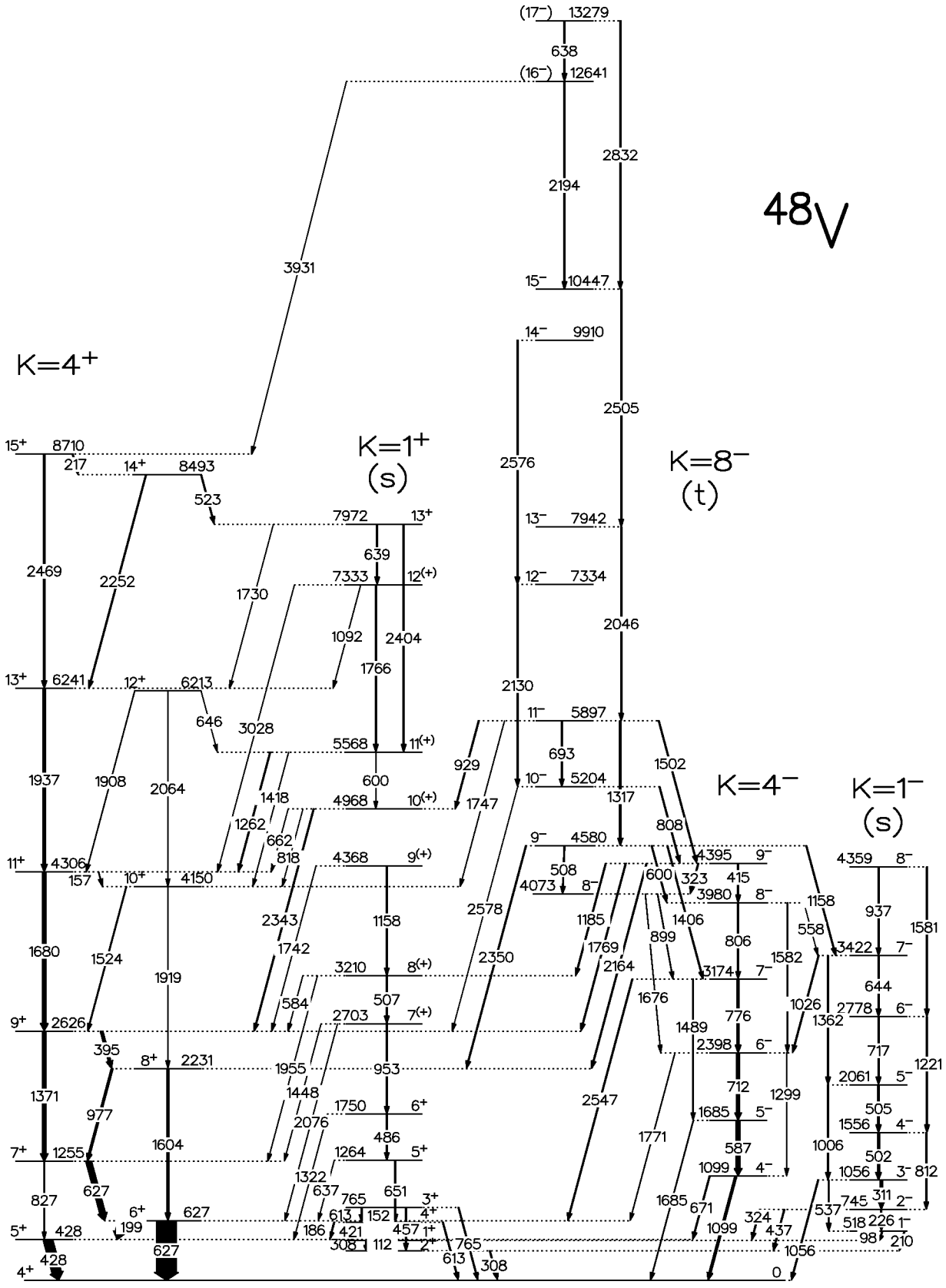

FIG. 1. Experimental decay scheme of the nucleus ^{48}V deduced from the present work.

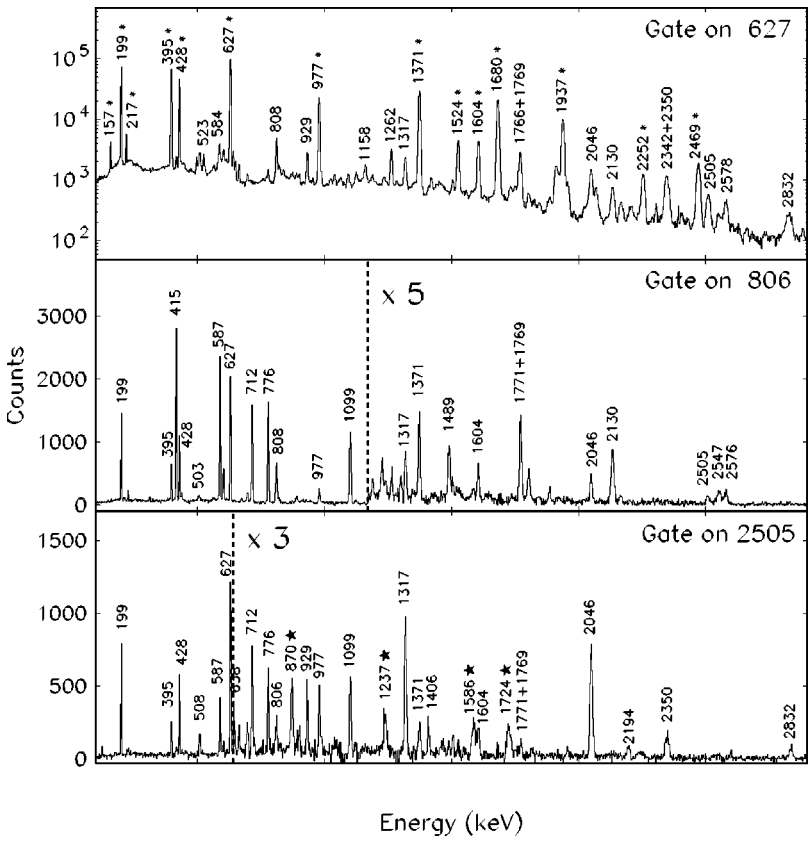

FIG. 2. (a) γ spectrum in coincidence with the 627 keV doublet and with three protons detected by the ISIS array. Transitions in the ground-state bands are labeled with an asterisk. Also the $14^+ \rightarrow 13_2^-$ 523 keV transition is clearly seen. (b) The same in coincidence with the $8^- \rightarrow 7^-$ 806 keV line. (c) The same in coincidence with the $15^- \rightarrow 13^-$ 2505 keV line. Stars denote lines of the ground-state band in ^{45}Sc, which are coincident with a line contained in the gate.

shown in Fig. 4, the agreement is rather good, in spite of the truncation made. The staggering of the $K^\pi = 1^-$ band is well reproduced. One may observe, however, that the $K^\pi = 8^-$ band is calculated about 500 keV lower than the experimental result, while the $K^\pi = 4^-$ band differs by only about 200 keV. The poor agreement for the level energy of the $K^\pi = 8^-$ band and of high-spin levels in general can be probably related to the truncation made in the calculations. The theoretical assignment of levels to the $K^\pi = 1^-$ and $K^\pi = 4^-$ bands above the backbending is rather arbitrary because of the large predicted configuration mixing. Notice that the two bands are already mixed at $I^\pi = 7^-$, as indicated by the intraband transitions. The $K^\pi = 8^-$ assignment to the observed high-spin band is confirmed by the large calculated $B(E2)$ values for the $\Delta I = 1$ transition. The signature splitting is rather well reproduced at low spins. At higher spins the agreement becomes worse.

It is interesting to observe that nearly all the levels known so far below 3 MeV excitation energy can be arranged within the four bands: $K^\pi = 4^+$, 1^+, 4^-, and 1^-.

In Tables I, II, and III the calculated $B(E2)$ and $B(M1)$ reduced strengths are reported, as well as the calculated branching ratios. In calculating $B(E2)$ values, the standard additive effective charge of 0.5 was assumed for both protons and neutrons, while the bare g factors were used in calculating the $B(M1)$ values. The theoretical branching ratios do not account for $E1$ decay-out, since $B(E1)$ values are not yet implemented in the code.

V. LIFETIME MEASUREMENTS

For the lifetime measurements, data from the thick target experiment were sorted into seven γ-γ matrices having on the first axis the signals from the detectors in rings at 34°, 60°, 72°, 90°, 108°, 120°, and 146° and on the second axis any of the other 39 detectors.

The program LINESHAPE [16] was modified in order to implement the NGTB procedure [6]. Shortly, the lifetime is obtained using an upper coincident transition as a probe and comparing the partly suppressed line shape (lower part of Fig. 5), obtained with a narrow gate on the transition to be studied, with the full line shape (upper part of Fig. 5) of the upper coincident transition. About two-thirds of the lifetimes of 25 states were obtained with the NGTB procedure. The stopping power tabulated by Northcliffe and Schilling [17], corrected for atomic shell effects [18], was used. More details about the analysis procedure are reported in Ref. [2], where also the accuracy of the stopping power is discussed.

The statistics obtained in the measurement with lead as backing material was more than a factor of 2 lower than that using gold, but it was important in order to extend the lifetime measurement to the low-lying members of the $K^\pi = 1^-$ band.

VI. DISCUSSION

A. Ground-state band

An example of NGTB analysis for the positive-parity yrast band is shown in Fig. 5. It should be noted that most of the observed transitions have a very pronounced line shape. As reported in Table I and also shown in Fig. 6 for an easier comparison, the deduced $B(M1)$ rate is very large for the $15^+ \rightarrow 14^+$ transition and shows a staggering down to low spins, which is accompanied by a smooth behavior of the

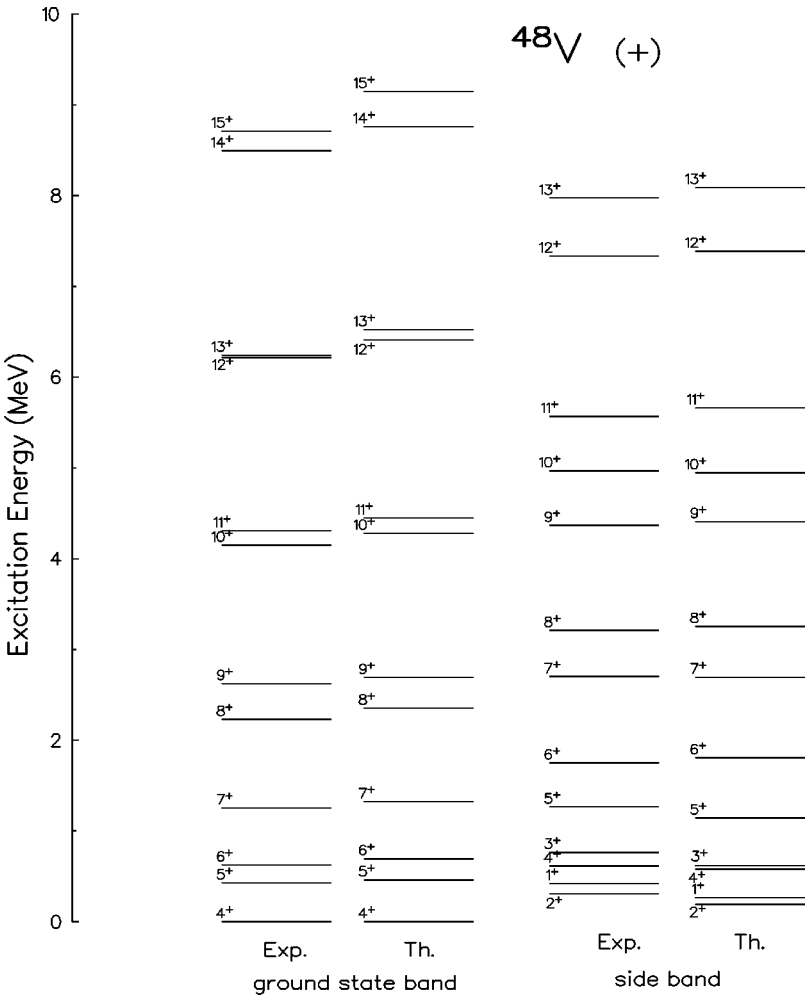

FIG. 3. Comparison of experimental energies for the positive-parity levels and LSSM calculated energies using the KB3G effective interaction.

$B(E2)$ values. Such a staggering behavior is an effect related to the $1f_{7/2}^{n}$ configuration space. In fact, in this space an even bigger staggering is predicted at low spins [19]. In the present case, configuration mixing dumps the staggering to a certain extent. The lifetime of the 10^{+} and 12^{+} yrast states could not be measured because of the statistics, being more than two orders of magnitude lower. The corresponding $B(M1)$ values, marked with stars in Fig. 6, were obtained by assuming the theoretical $B(E2)$ values for the $\Delta I=2$ branches. This assumption relies on the fact that $B(E2)$ values for natural-parity yrast levels are generally well predicted by the LSSM in the middle of the $1f_{/2}$ shell. Such reference values are taken with a conservative 50% error.

Only an upper limit was given for the lifetime of the 14^{+} state. One observes, however, that the $B(M1)$ value of the transition to the yrast 13^{+} level is about 14 times smaller than that to the yrare one. Assuming an upper limit of $4\mu_N^2$ for the former, an upper limit of $0.3\mu_N^2$ for the latter value is obtained.

From the $B(E2)$ values of lower states we extract a quadrupole deformation parameter $\beta\cong 0.21$, under the assumption of a $K^{\pi}=4^{+}$ band. This value is much smaller than that observed in ^{48}Cr: namely, $\beta\cong 0.3$. The discrepancy might be explained taking into consideration triaxiality with positive value of γ, as suggested for ^{46}V [20], giving rise to smaller $B(E2)$ values. Also the observed signature splitting points to triaxiality.

Few mixing ratios are reported in the literature for the $\Delta I=1$ intraband transitions [12]. They are significantly different from zero for the $6^{+}\rightarrow 5^{+}$ 199 keV and $8^{+}\rightarrow 7^{+}$ 977 keV transitions. The multipole mixing ratio for the former is $\delta=0.14(2)$, giving a $B(E2)$ rate consistent with theory. The value for the second transition is $\delta=0.34(4)$, giving rise to a very large $B(E2)=325(60)\ e^2\,\mathrm{fm}^4$, in disagreement with the theoretical expectations. In order to check this point, the γ-ray angular distribution of the 977 keV line, gating on the 395 feeding transition, was evaluated, which turned out to have a typical dipole behavior, with $|\delta|<0.10$.

Calculations succeed in explaining very peculiar facets, such as the decay of the yrast 14^{+} level toward the yrare 13_s^{+}.

B. Positive-parity sideband

In Table II, the comparison is extended to transitions depopulating the yrare band states. Only the comparison with theoretical branching ratios is considered because lifetime measurements were not possible, given the low statistics. Strictly speaking, the parity of this band is not fully experimentally established, but the outstanding agreement with

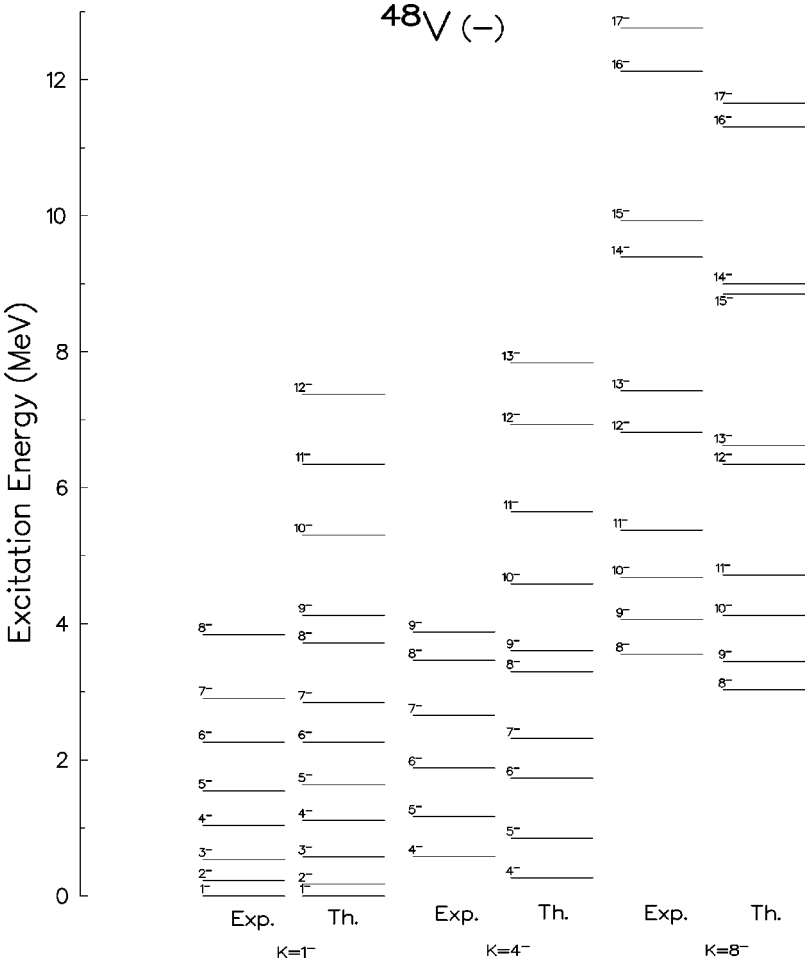

FIG. 4. Same as Fig. 3 for the negative-parity levels.

theory is encouraging. The complex decay pattern of the yrare 13^+ level is well described. Even for this state, which is essentially not deformed, the effect of configuration mixing is decisive. In fact, the branching ratios of the upper levels are not well predicted in the $1f_{7/2}^n$ configuration space [19]. The complex branching ratios for all transitions in this band are reasonably well predicted, with a few notable exceptions. For example, the $5_s^+ \rightarrow 4^+$ transition was not observed, while it is predicted to have a branching ratio of 15%. The calculated $B(M1)$ value is, however, only $0.057\mu_N^2$ and it is not surprising that small values can have large relative errors. It is also a success of the LSSM, the fact that the branching ratio of the $10_s^+ \rightarrow 9_s^+$ is predicted to be very small, in agreement with the experimental limit. Unfortunately, there is no experimental estimate of the deformation of the positive-parity sideband at low spins, but in virtue of the excellent LSSM predictions for the level energies, one is encouraged to rely on the theoretical predictions for the reduced rates. Calculations show that the $B(E2)$ values are consistent with a deformation similar to that of the g.s. band. The stretched $E2$ branches are predicted to be small because of the enhancement of the competing $M1$ transitions. The stretched interband $B(E2)$ values, which are not reported, would be in every case less than 1 $e^2\,\mathrm{fm}^4$, indicating the validity of the K selection rule.

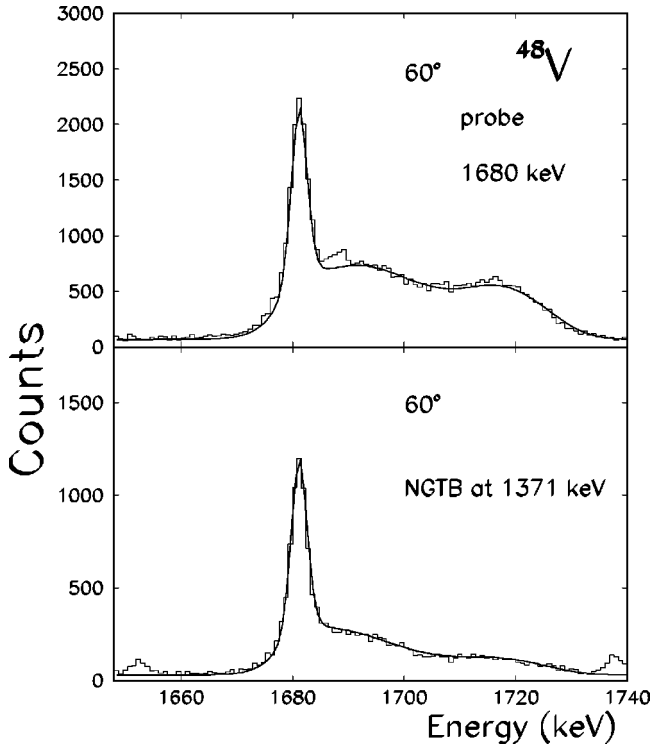

FIG. 5. NGTB analysis for the $9^+ \rightarrow 7^+$ 1371 keV transition, using the 1681 keV line as a probe.

TABLE I. Results for the ground-state positive-parity band in ^{48}V. Transitions in brackets were not observed. Theoretical branches less than 0.5% are set to 0. Experimental $B(M1)$ with asterisk were calculated using the theoretical value of $B(E2)$ for the $\Delta I=2$ $E2$ branch.

Transition	E_γ Expt. (keV)	E_γ SM (keV)	Int	BR Expt. (%)	BR SM (%)	τ Expt. (ps)	$B(E2)$ Expt. (e^2 fm^4)	$B(E2)$ Th. (e^2 fm^4)	$B(M1)$ Expt. (μ_N^2)	$B(M1)$ Th. (μ_N^2)
$5\rightarrow4$	427.8(4)	490	100	100	100	8.8(14)[a]		216	0.12(2)	0.172
$6\rightarrow4$	627.2(3)	704	110	57(5)	60	108(9)[a]	67(8)	52		
$6\rightarrow5$	199.3(2)	213	87	43(5)	40		300(120)	198	0.039(5)	0.032
$7\rightarrow5$	826.5(3)	875	3	2.0(3)	1	0.60(15)[b,c]	40(13)	60		
$7\rightarrow6$	627.4(4)	662	160	98.0(3)	99			146	0.45(11)	0.536
$8\rightarrow6$	1604.2(4)	1765	42	46(3)	57	0.31(5)[b,c]	117(17)	116		
$8\rightarrow7$	976.6(4)	1103	50	54(3)	43			65	0.080(20)	0.075
$9\rightarrow7$	1371.4(4)	1438	110	55(3)	55	0.80(12)[c]	124(16)	140		
$9\rightarrow8$	394.9(4)	335	91	45(3)	45			91	0.50(8)	0.597
$10\rightarrow8$	1918.5(8)	2046	3.5	22(5)	24			120		
$10\rightarrow9$	1523.5(8)	1711	26	78(5)	76			44	0.10(5)*	0.227
$10\rightarrow8_s$	(941)	1027	-	<2	0			4.2		
$11\rightarrow9$	1680.3(4)	1819	120	97.0(6)	98	0.52(6)[c]	115(15)	132		
$11\rightarrow10$	157.0(4)	108	3.6	3.0(6)	2			37	0.65(15)	0.660
$12\rightarrow10$	2064.0(8)	2233	3.6	33(6)	40			91		
$12\rightarrow11$	1908.4(8)	2175	9	54(6)	48			20	0.10(5)*	0.043
$12\rightarrow10_s$	(1246)	1463	-	<2	0			0.2		
$12\rightarrow11_s$	646.0(8)	748	1.8	13(4)	12			2.6		0.252
$13\rightarrow11$	1937(1)	2172	92	100	100	0.28(4)	106(15)	104		
$13\rightarrow12$	(28)	112	-	<3	0			23		0.748
$13\rightarrow11_s$	(674)	860	-	<3	0			0.2		
$14\rightarrow12$	(2280)	2350	-	<4	3			16		
$14\rightarrow13$	2252(1)	2305	11	85(3)	86	<0.10		0.3	0.07–0.3	0.198
$14\rightarrow12_s$	(1161)	1372	-	<3	0			28		
$14\rightarrow13_s$	522.8(8)	638	1.9	15(3)	10			23	>0.60	1.32
$15\rightarrow13$	2469(1)	2700	23	88(2)	92	0.17(4)	38(9)	46		
$15\rightarrow14$	217.1(5)	388	3.6	12(2)	8			13	3.3(9)	2.71
$15\rightarrow13_s$	(739)	1057	-	<3	0			16		

[a]Reference [12].
[b]Only the partner was analyzed.
[c]Also NGTB procedure.

C. Negative-parity states

Examples of line shapes are shown in Figs. 7, 8, and 9 for the three negative-parity bands $K^\pi=4^-$, $K^\pi=1^-$, and $K^\pi=8^-$, respectively. The upper members of the $K^\pi=1^-$ band are very broadened so that the standard analysis is more convenient, as shown in Fig. 8. Lifetime measurements allowed the assignment of $M1$ character to some dipole transitions. As in previous papers [3–5], the recommended upper limit of 3×10^{-4} Weisskopf unit (W.u.) was assumed for the $E1$ strengths [3]. Assuming a parity change, the $E1$ strengths for the $9\rightarrow8^-$ 415 keV, $10_t\rightarrow9^-$ 808 keV, and $9_t\rightarrow8^-$ 508 keV transitions would be too large, being, respectively, $5(1)\times10^{-3}$, $4(1)\times10^{-3}$, and $2.0(5)\times10^{-3}$ W.u. We thus assign negative parity to the decaying levels. Both negative-parity bands $K^\pi=1^-$ and $K^\pi=4^-$ have little signature splitting, which suggests small triaxiality. They can be described at low spin with a deformation parameter $\beta\simeq0.26$, giving rise to a shape coexistence between bands of different parity, as observed for other nuclei such as the neighbor ^{47}V [4]. As shown in Table III, satisfactory agreement is obtained for

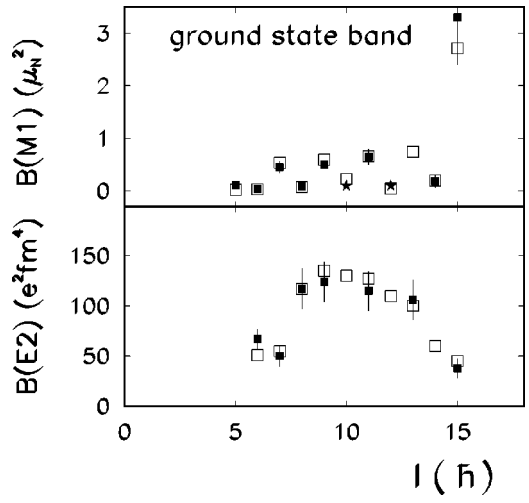

FIG. 6. Reduced transition rates for the yrast positive-parity states in ^{48}V, compared with the theoretical predictions. Stars refer to $M1$ values normalized to theoretical $B(E2)$ values of the $\Delta I^\pi=2$ branches, as discussed in the text.

TABLE II. Results for the positive-parity sideband in ^{48}V. Transitions in brackets were not observed. Theoretical branches less than 0.5% are set to 0.

Transition	E_γ Expt. (keV)	E_γ SM (keV)	Int	BR Expt. (%)	BR SM (%)	τ Expt. (ps)	$B(E2)$ Expt. (e^2 fm^4)	$B(E2)$ Th. (e^2 fm^4)	$B(M1)$ Expt. (μ_N^2)	$B(M1)$ Th. (μ_N^2)
$2_s \rightarrow 4$	308.3(1)	193	9	100		10 260(60)[a]	29.1(2)	24		
$1_s \rightarrow 2_s$	112.4(1)	72	3.5	100		<1400		352		3.01
$4_s \rightarrow 4$	613.4(1)	578	0.17	89(2)	89	21.6(11)[a]	62(25)	27	0.009(1)[a]	0.009
$4_s \rightarrow 5$	185.5(1)	118	0.02	11(2)	10			23	0.045(8)[a]	0.035
$4_s \rightarrow 2_s$	(305)	385	-	<5	1			125		
$3_s \rightarrow 4$	764.9(1)	618	-	44.1(22)[a]	50			0.1		0.26
$3_s \rightarrow 2_s$	456.7(1)	425	-	53.8(22)[a]	49			96		1.56
$3_s \rightarrow 1_s$	(344)	350	-	<2	0			126		
$3_s \rightarrow 4_s$	151.7(2)	40	-	2.2(3)[a]	1			56		1.09
$5_s \rightarrow 4$	(1264)	1142	-	<5	14			0.5		0.057
$5_s \rightarrow 4_s$	651.2(2)	564	0.17	79(5)	66			41		1.90
$5_s \rightarrow 3_s$	(499)	524	-	<5	0			164		
$5_s \rightarrow 5$	(836)	681	-	<5	5			0.1		0.058
$5_s \rightarrow 6$	637.3(2)	447	0.04	21(5)	15			3.6		0.459
$6_s \rightarrow 4_s$	(1137)	1228	-	<6	2			96		
$6_s \rightarrow 5$	1322(1)	1346	0.56	85(6)	87			36		0.32
$6_s \rightarrow 6$	(1124)	1112	-	<5	1			2.2		0.008
$6_s \rightarrow 5_s$	486(1)	665	0.10	15(6)	10			30		0.77
$7_s \rightarrow 5$	(2334)	2235	-	<6	5			8.4		
$7_s \rightarrow 5_s$	(1438)	1553	-	<6	6			109		
$7_s \rightarrow 6$	2076(1)	2000	0.21	26(5)	38			8.2		0.031
$7_s \rightarrow 7$	1448(1)	1373	0.09	11(4)	4			5.2		0.010
$7_s \rightarrow 6_s$	953(1)	889	0.50	63(6)	47			21		0.371
$8_s \rightarrow 6_s$	(1459)	1447		<10	13			116		
$8_s \rightarrow 7$	1955(1)	1932	0.40	39(7)	7			15		0.004
$8_s \rightarrow 7_s$	507(1)	559	0.30	28(6)	32			45		0.979
$8_s \rightarrow 8$	(979)	902	-	<10	7			0.2		0.028
$8_s \rightarrow 9$	584(1)	562	0.35	33(7)	41			3.2		0.842
$9_s \rightarrow 7_s$	(1665)	1714	-	<10	6			61		
$9_s \rightarrow 8$	(2137)	2057	-	<15	14			1.2		0.013
$9_s \rightarrow 8_s$	1158(1)	1155	0.2	55(7)	55			3.2		0.316
$9_s \rightarrow 9$	1742(1)	1716	0.2	45(7)	25			1.5		0.043
$10_s \rightarrow 9$	2343(1)	2255	2.0	86(9)	78			6		0.082
$10_s \rightarrow 8_s$	(1759)	1693	-	<6	1			13		
$10_s \rightarrow 9_s$	(601)	538	-	<6	0			0.05		0.007
$10_s \rightarrow 10$	818(1)	666	0.2	9(2)	13			7.4		0.324
$10_s \rightarrow 11$	662(1)	500	0.1	5(2)	7			3.2		0.327
$11_s \rightarrow 9_s$	(1201)	1253	-	<5	0			24		
$11_s \rightarrow 10$	1418(1)	1381	0.5	20(6)	12			1.7		0.098
$11_s \rightarrow 11$	1262(1)	1215	1.5	60(8)	76			7.0		0.904
$11_s \rightarrow 10_s$	600(1)	715	0.5	20(6)	11			43		1.154
$12_s \rightarrow 11$	3028(2)	2941	0.3	12(3)	0			0.6		0.001
$12_s \rightarrow 12$	(1119)	978	-	<7	7			1.9		0.145
$12_s \rightarrow 13$	1092(1)	866	0.6	16(4)	15			6.3		0.347
$12_s \rightarrow 10_s$	(2365)	2441	-	<5	8			42		
$12_s \rightarrow 11_s$	1766(1)	1726	1.6	72(8)	70			17		0.369
$13_s \rightarrow 12$	(1759)	1680	-	<5	1			0.6		0.002
$13_s \rightarrow 13$	1730(1)	1568	1.0	30(5)	31			3.2		0.063
$13_s \rightarrow 11_s$	2404(1)	2428	0.5	15(5)	24			46		
$13_s \rightarrow 12_s$	639(1)	702	1.8	55(6)	43	<0.20		30		1.74

[a]Reference [12].

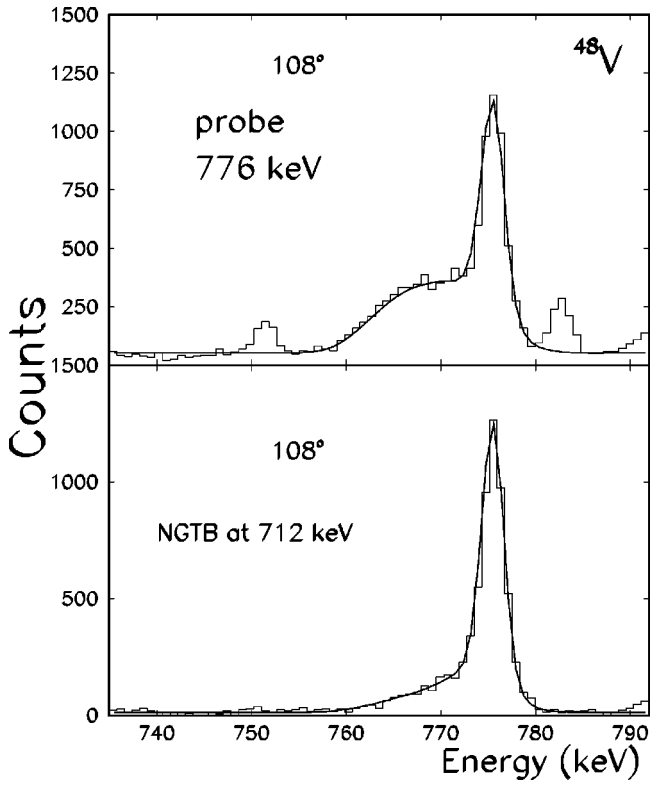

FIG. 7. NGTB analysis for the $6^- \rightarrow 5^-$ 712 keV transition, using the 776 keV transition as a probe.

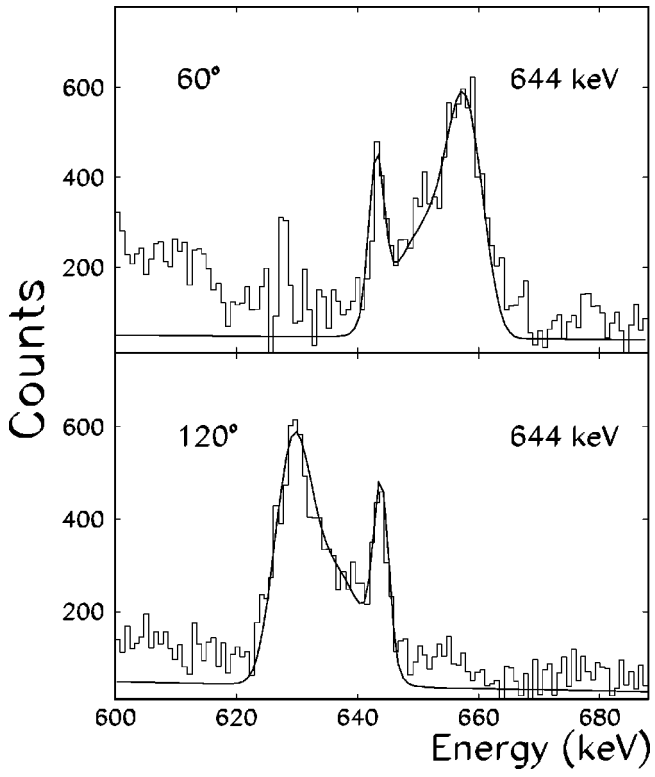

FIG. 8. Standard DSAM analysis for the $7_s^- \rightarrow 6_s^-$ 644 keV transition observed at 60° and 120°.

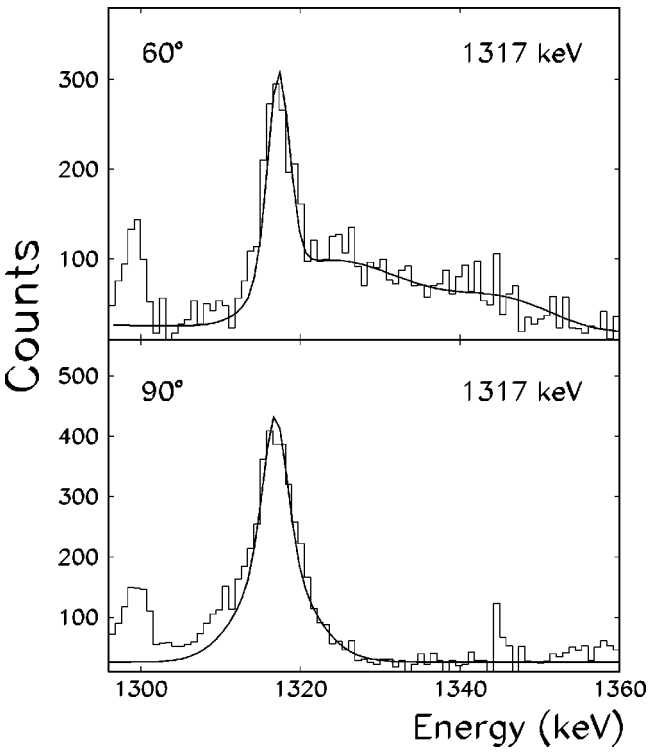

FIG. 9. Standard DSAM analysis for the $11_t^- \rightarrow 9_t^-$ 1317 keV transition observed at 60° and 90°.

these two bands below the 8^- levels. It is noticeable that the $B(M1)$ strength of the $7_s^- \rightarrow 6^-$ interband transition is correctly predicted. Disagreement occurs for the transitions from the two lower 8^- levels. This is due to the large calculated negative-energy offset for the $K^\pi = 8^-$ band, splitting the two levels with a reduced configuration mixing. The consequent energy inversion is suggested by the theoretical $B(E2)$ values. On the contrary, the two lower 9^- states are apparently not strongly mixed, as the decay from the yrast 11^- proceeds mostly to the yrare 9^-, while two similar $B(E2)$ values are predicted for its decay to two lower mixed 9^- states. Poor agreement is obtained near the band crossing, while agreement is restored above the 10^- level. The $B(M1)$ values are correctly predicted for the $K^\pi = 8^-$ band: i.e., to be small, save for transitions approaching the band termination, as shown in Table III. A similar behavior was observed also in the unnatural parity side band in ^{47}V and has to be related to the alignment of all spins at the band termination.

It is particularly worth noticing the good reproduction of the decay of the 17^- yrast level, which is the band termination in $2d_{3/2}^{-1} \otimes 1f_{7/2}^{n+1}$ configuration space. An anomaly is, however, observed: the $B(E2)$ value of the $16^- \rightarrow 14^-$ 2731 keV transition is predicted to be very small, in disagreement with a description as an intraband transition. We note that two close-lying 14^- levels are predicted, which may interfere.

Reduced transition rates, before and after the band crossing, are displayed in Fig. 10.

D. $E1$ transitions

Finally, in Table IV several $E1$ strengths are presented, which could be determined for the transitions depopulating

TABLE III. Results for the negative-parity sidebands in ^{48}V. Gammas in brackets were not observed. Theoretical branches less than 0.5% are set to 0.

Transition	E_γ Expt. (keV)	E_γ SM (keV)	Int	BR Expt. (%)	BR SM (%)	τ Expt. (ps)	$B(E2)$ Expt. (e^2 fm^4)	$B(E2)$ Th. (e^2 fm^4)	$B(M1)$ Expt. (μ_N^2)	$B(M1)$ Th. (μ_N^2)
$2_s \rightarrow 1_s$	226.3(1)	172	9.0	92(2)	100	24.9(26)[a]		378	0.120(14)	0.214
$3_s \rightarrow 1_s$	537.2(1)	573	0.5	5(1)	7	4.5(11)[a]	195(61)	218		
$3_s \rightarrow 2_s$	310.8(1)	401	8.0	89(3)	93			190	0.378(95)	0.306
$4_s \rightarrow 2_s$	812.4(2)	941	1.1	15(3)	14	1.4(4)[b,c,d]	248(86)	304		
$4_s \rightarrow 3_s$	501.7(1)	540	7.0	85(3)	86			82	0.274(79)	0.351
$5_s \rightarrow 3_s$	1006.2(3)	1062	1.0	35(5)	30	1.1(3)[b,c,d]	253(95)	298		
$5_s \rightarrow 4_s$	504.7(3)	540	6.1	65(5)	70			45	0.264(64)	0.391
$6_s \rightarrow 4_s$	1221.1(3)	1150	1.5	28(5)	33	0.28(4)[b,c]	301(69)	342		
$6_s \rightarrow 5_s$	717.1(4)	628	5.3	72(5)	67			15	0.397(64)	0.371
$7_s \rightarrow 5_s$	1362(5)	1207	1.5	30(5)	31	0.19(4)[b,c]	275(74)	258		
$7_s \rightarrow 6_s$	643.6(4)	579	2.1	35(6)	32			5.2	0.393(106)	0.327
$7_s \rightarrow 6$	1026.1(6)	1112	2.1	35(6)	37			33	0.090(24)	0.091
$8_s \rightarrow 6_s$	1581.3(6)	1456	1.1	46(6)	35	0.12(4)[b,c]	316(113)	290		
$8_s \rightarrow 7_s$	937.4(6)	877	1.4	54(6)	65			1.0	0.312(110)	0.484
$5 \rightarrow 4$	586.5(4)	581	19	91(2)	100	0.86(10)[b]		380	0.299(36)	0.190
$6 \rightarrow 4$	1299.3(4)	1462	1.2	6.8(13)	10	0.32(3)[b,c]	49(22)	82		
$6 \rightarrow 5$	712.4(4)	881	15	86.6(15)	90			376	0.423(44)	0.502
$7 \rightarrow 5$	1489.0(4)	1461	4	22(4)	24	0.20(2)[b,c]	122(24)	174		
$7 \rightarrow 6$	775.7(4)	580	11	71(4)	76			326	0.430(46)	0.593
$8 \rightarrow 6$	1582.3(4)	1571	4	30(4)	51	0.22(3)[b,c]	112(19)	38		
$8 \rightarrow 7$	806.4(4)	718	9	68(5)	45			19	0.335(43)	0.163
$8 \rightarrow 7_s$	558(1)	186	11	2.1(6)	4			46	0.030(9)	0.040
$9 \rightarrow 7$	(1222)	1139	-	<5	46	1.3(2)[b,c,d]	<11	73		
$9 \rightarrow 8$	414.5(4)	421	4	57(4)	24			143	0.349(59)	0.099
$9 \rightarrow 8_t$	323(1)	148	0.4	5(2)	30			1.3	0.065(27)	0.266
$8_t \rightarrow 6$	1676(1)	1571	1.6	38(5)	29	0.14(4)[b,c]	167(52)	140		
$8_t \rightarrow 7$	898.9(5)	991	3.0	62(5)	71			220	0.349(103)	0.580
$9_t \rightarrow 7$	1406.4(5)	1294	3	34(5)	31	0.56(7)[b,c]	90(17)	67		
$9_t \rightarrow 8$	600.0(4)	576	2	27(4)	21			23	0.127(25)	0.081
$9_t \rightarrow 8_t$	507.7(4)	303	1.5	20(4)	42			15	0.155(36)	0.271
$9_t \rightarrow 7_s$	1158.2(5)	762	0.2	2.7(6)	6		16(5)	36		
$10_t \rightarrow 8$	(1224)	1186	-	<5	4	0.40(10)		43		
$10_t \rightarrow 8_t$	(1132)	912	-	<5	1			12		
$10_t \rightarrow 9_t$	(623)	610	-	<5	13			6	<0.03	0.121
$10_t \rightarrow 9$	807.9(5)	764	4	95(2)	82			136	0.242(60)	0.363
$11_t \rightarrow 9$	1502(1)	1271	0.4	6(2)	74	0.9(1)	7(2)	105		
$11_t \rightarrow 9_t$	1317.0(4)	1116	3	55(7)	26		125(21)	71		
$11_t \rightarrow 10_t$	693.4(8)	506	0.8	13(3)	0			105	0.024(6)	0.001
$12_t \rightarrow 10_t$	2130(1)	2170	2.1	100	92	0.17(3)	109(19)	80		
$12_t \rightarrow 11_t$	(1437)	1664	-	<10	8			54	<0.01	0.007
$13_t \rightarrow 11_t$	2046(1)	1902	0.5	100	100	0.13(2)	175(27)	184		
$13_t \rightarrow 12_t$	(608)	239	-	<4	0			98	<0.08	0.002
$14_t \rightarrow 12_t$	2576(2)	2612	0.5	100	100	<0.08	>90	96		
$14_t \rightarrow 13_t$	(1968)	2374	-	<8	0			96		0.002
$15_t \rightarrow 13_t$	2505(2)	2225	1.5	100	100	<0.08	>100	120		
$16_t \rightarrow 14_t$	(2731)	2311	-	<10	0			3		
$16_t \rightarrow 15_t$	2194(1)	2459	1.0	50(20)	100			8		0.371
$17_t \rightarrow 15_t$	2832(2)	2804	1.1	80(10)	63			81		
$17_t \rightarrow 16_t$	638(1)	345	0.3	20(10)	37			5		2.322

[a]Reference [12].

[b]Only the partner line was analyzed.

[c]Also NGTB.

[d]Value using the target with lead backing.

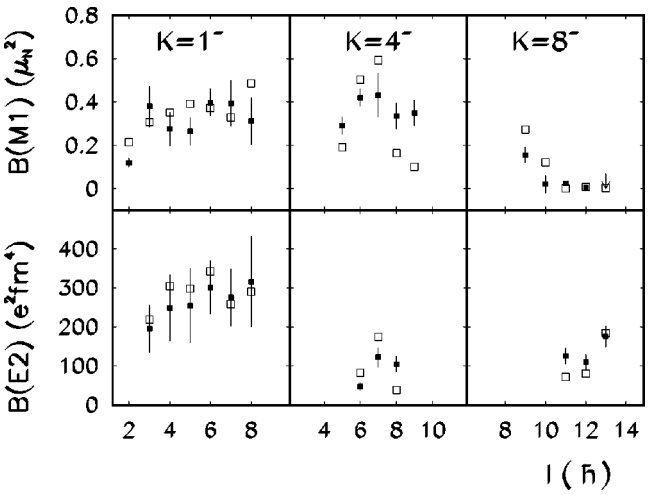

FIG. 10. Reduced transition rates for the negative-parity states in ^{48}V, compared with theoretical predictions. Solid squares are experimental values and open squares are the predictions, for $K^\pi = 1^-$, $K^\pi = 4^-$, and $K^\pi = 8^-$ bands, respectively.

negative-parity levels towards positive-parity levels. They are in general much retarded with respect to the upper limit of 3×10^{-4} W.u. The fastest is the $11_t^- \rightarrow 10_s^+$ 929 keV transition, which is calculated to have an $E1$ strength of $2.0(4)\times10^{-4}$ W.u.

VII. CONCLUSIONS

A detailed spectroscopic investigation for the nucleus ^{48}V is presented. The observed levels are grouped in five bands, classified with $K^\pi = 4^+$, 1^+, 4^-, 1^-, and 8^-, respectively, which are labeled with Nilsson configurations. The similarity with ^{46}V should be noticed, where also five bands of similar nature have been observed [5]. The major difference between ^{46}V and ^{48}V is that in ^{46}V both the unpaired neutron and proton occupy the same $[321]3/2^-$ orbital, while in ^{48}V the last neutron occupies the $[312]5/2^-$ one. This implies that in the $N=Z$ nucleus ^{46}V the $1d_{3/2}$ hole is 50% a proton and 50% a neutron excitation. On the other hand, the unnatural-parity bands in ^{48}V originate from a proton hole in the $1d_{3/2}$ orbital.

In ^{48}V two positive-parity bands with $K^\pi = 4^+$ and 1^+ originate, while in ^{46}V they have $K^\pi = 3^+$ and 0^+, respectively. Similarly, the excitation of a nucleon from the $d_{3/2}$ $[202]3/2^+$ orbital to the next available orbital gives rise in ^{46}V to $K^\pi = 3^-$ and 0^- bands, which should be compared with the $K^\pi = 4^-$ and 1^- partners in ^{48}V. Finally, in ^{46}V the excitation from the $[202]3/2^+$ orbital to the first empty orbital, followed by the parallel coupling of the four unpaired nucleons, gives rise to a $K^\pi = 7^-$ band, while in ^{48}V a $K^\pi = 8^-$ band is obtained.

In ^{48}V all of the observed spectroscopic quantities for positive-parity states are in excellent agreement with LSSM calculations in full *pf* configuration space. The decays from the spherical high-spin states do not obey the K selection rules. The agreement of the calculated reduced transition rates for the negative-parity levels is reasonably good, considering the truncation of the model space. The theoretical description of levels fails around the region of band crossing between the $K^\pi = 4^-$ and $K^\pi = 8^-$ bands.

TABLE IV. Results for $E1$ transitions in ^{48}V.

Transition	E_q (keV)	Int	BR (%)	τ (ps)	W.u. (10^{-5})
$1_s^- \rightarrow 2^+$	210.3(1)	6.5	66(7)	3924(87)[a]	1.5
$1_s^- \rightarrow 1^+$	97.7(1)	3.5	34(7)		6.5
$2_s^- \rightarrow 2^+$	436.6(1)	0.5	4.9(9)	24.9(26)[a]	1.7
$2_s^- \rightarrow 1^+$	324.3(1)	0.3	3.1(8)		2.7
$3_s^- \rightarrow 4^+$	1056.1(4)	0.5	5(2)	4.5(11)[a]	3.1
$4^- \rightarrow 4^+$	1099.2(4)	20	96.1(9)	6.5(6)[a]	8.2
$4^- \rightarrow 5^+$	671.2(4)	0.9	3.9(9)	”	1.5
$5^- \rightarrow 4^+$	1685.3(4)	1.9	9.1(17)	0.86(8)	1.6
$6^- \rightarrow 6^+$	1771.2(4)	1.1	6.6(11)	0.32(3)	2.7
$7^- \rightarrow 6^+$	2547.4(6)	1.2	6.5(2)	0.20(2)	1.5
$9^- \rightarrow 8^+$	2164.4(4)	0.3	3.8(9)	1.3(2)	0.2
$9^- \rightarrow 9^+$	1769.3(4)	2.5	35.5(30)	”	3.6
$9^- \rightarrow 8_s^+$	1185.4(5)	0.1	0.7(3)	”	0.2
$9_t^- \rightarrow 8^+$	2349.5(6)	1.9	17(4)	0.56(4)	1.7
$10_t^- \rightarrow 9^+$	2578(1)	0.2	5(2)	0.40(10)	0.5
$11_t^- \rightarrow 10^+$	1747(1)	0.3	5.0(9)	0.9(1)	0.8
$11_t^- \rightarrow 10_s^+$	929(1)	1.1	19.8(40)	”	20

[a]Reference [12].

ACKNOWLEDGMENTS

R.V.R. and N.H.M. would like to acknowledge financial support from the Brazilian agency CNPq (Conselho Nacional de Desenvolvimento Científico e Tecnológico) and INFN (Italy). A.P. and J.S.-S. are supported by the Spanish Ministry of Science and Technology under Grant No. BFM2000-30. The CCCFC (UAM) Spain provided part of the computer cycles employed in this work. A.G. was supported by the EC under Contract No. ERBCHBGCT940713.

[1] S. M. Lenzi *et al.*, Z. Phys. A **354**, 117 (1996).
[2] F. Brandolini *et al.*, Nucl. Phys. **A642**, 387 (1998).
[3] F. Brandolini *et al.*, Phys. Rev. C **60**, 041305 (1999).
[4] F. Brandolini *et al.*, Nucl. Phys. **A693**, 517 (2001).
[5] F. Brandolini *et al.*, Phys. Rev. C **64**, 044307 (2001).
[6] F. Brandolini and R. V. Ribas, Nucl. Instrum. Methods Phys. Res. A **417**, 150 (1998).
[7] E. Caurier *et al.*, Phys. Rev. C **50**, 225 (1994).
[8] E. Caurier *et al.*, Phys. Rev. Lett. **75**, 2466 (1995).
[9] G. Martinez-Pinedo *et al.*, Phys. Rev. C **54**, R2150 (1996).
[10] G. Martinez-Pinedo *et al.*, Phys. Rev. C **55**, 187 (1997).
[11] A. Poves and J. Sanchez-Solano, Phys. Rev. C **58**, 179 (1998).
[12] T. W. Burrows, Nucl. Data Sheets **68**, 1 (1993).
[13] J. Cameron *et al.*, Phys. Rev. C **49**, 1347 (1994).

[14] M. Hasegawa *et al.*, Nucl. Phys. **A674**, 411 (2000).
[15] A. Poves *et al.*, Nucl. Phys. **A694**, 157 (2001).
[16] J. C. Wells and N. Johnson, Report No. ORNL-6689, 1991, p. 44.
[17] L. C. Northcliffe and R. F. Schilling, Nucl. Data Tables A **7**, 233 (1976).
[18] S. H. Sie *et al.*, Nucl. Phys. **A291**, 11 (1977).
[19] W. Kutschera, B. A. Brown, and K. Ogawa, Riv. Nuovo Cimento **1**, 12 (1978).
[20] C. D. O'Leary *et al.*, Phys. Lett. B **459**, 73 (1999).